AD-776 413

THE STRUCTURE OF NON-CRYSTALLINE MATERIALS

Farrel W. Lytle

Boeing Company

Prepared for:

Army Research Office-Durham
Advanced Research Projects Agency

31 December 1973

DISTRIBUTED BY:

NTIS
National Technical Information Service
U. S. DEPARTMENT OF COMMERCE
5285 Port Royal Road, Springfield Va. 22151

AQ0-9209. 8-Q

Form Approved
Budget Bureau No. 22-R0293

AD776413

Final Report, February 4, 1971 - December 31, 1973

THE STRUCTURE OF NON-CRYSTALLINE MATERIALS

Contract DAHC04 71 C 0010
Program Element Code: 61101D
ARPA Order No. 1562

[1974]

Principal Investigator
Farrel W. Lytle
(206) 655-5574
655-2954

The Boeing Company
Seattle, Washington

DISTRIBUTION STATEMENT A
Approved for public release;
Distribution Unlimited

DDC
RECEIVED
MAR 27 1974
B

Reproduced by
NATIONAL TECHNICAL
INFORMATION SERVICE
U S Department of Commerce
Springfield VA 22151

Amount: $180,428

61

Reproduced from best available copy.

Disclaimer

The views and conclusions contained in this document are those of the authors and should not be interpreted as necessarily representing the official policies, either expressed or implied, of the Advanced Research Projects Agency or the U. S. Government.

Summary of Research

The primary purpose of this research was to develop the phenomenon of extended x-ray absorption fine structure (EXAFS) as a technique for investigating the structure of non-crystalline materials, particularly amorphous semiconductors. A theory had been developed (Sayers, Lytle, Stern, "Advances in X-ray Analysis", Vol. 13, p. 248 (Plenum, New York, 1970) which treated EXAFS as a scattering of the ejected photoelectron by the near neighbors of the absorbing atom. Soon after the research began a major breakthrough was achieved in which the theoretical EXAFS expression and experimental data could be formally inverted into a radial structure function using the Fourier integral theorem.[1] The technique was further developed and applied to an investigation of the structures of Ge, GeO_2, and GeSe[2] to make the important point that the environment of all the different atoms in a multicomponent material could be determined. This work was recognized as a significant contribution to x-ray physics when Dale Sayers was awarded the 1972 Sidhu award by the Pittsburgh Diffraction Conference. Dr. Sayers' Ph.D. thesis, which described this work in detail was submitted as a special technical report.[3]

The surface-active character of evaporated amorphous germanium (E Ge) was emphasized in a calorimetric, diffraction and microscopic evaluation[4] which showed that 3 wt.% H_2O could be adsorbed when E Ge was exposed to air and could not all (50%) be removed unless the sample was heated above the recrystallization temperature. During recrystallization electron diffraction patterns showed transient (222) reflections (normally forbidden) which were interpreted as evidence of wurtzite-type bonding in the original material.

The EXAFS work on amorphous semiconductors was continued on GeSe, $GeSe_2$, As_2Se_3, As_2S_3, and As_2Te_3[5] and reported at the 1973 Conference on Amorphous Semiconductors at Garmisch-Partenkirchen. This work developed a normalization technique which allowed determination of absolute coordination numbers as well as identifying the kinds of atoms in the first coordination sphere. For example, in amorphous

As_2Se_3 we found the As atom to have 3 nearest neighbors (2Se and 1 As) while Se had 2 nearest neighbors (1 As and 1 Se).

The technique was also used to investigate impurity charge shielding[6] and determine atomic arrangement around the catalytic atoms in a supported catalyst[7]. The technique is finding great interest among catalyst chemists at a time when progress in this important energy-related field is in the national interest.

Accompanying this final report are three papers (which will be submitted for publication) describing the EXAFS experimental[8] and data analysis techniques[9,10]. These reports describe in detail our practice of the technique.

For the future of the technique, a proposal was made to NSF and a grant awarded to the University of Washington (Stern, Sayers, Lytle-consultant) to develop an EXAFS experiment at the Stanford Synchrotron Radiation Project. The x-ray intensity which can be obtained at this source is at least 10^5 greater than that of ordinary x-ray tubes and will allow data of higher resolution and better precision in a much shorter time.

Conclusions

In competition with x-ray, electron, or neutron scattering the EXAFS technique has the important advantage that the origin of the radial structure function (two body correlation function) is fixed at the site of the species-determined x-ray absorption event while all other techniques average over all the different kinds of atoms in the material. The results obtained on amorphous semiconductors are important and unique and will allow theorists to construct more accurate models of these materials. The catalyst work is only the top of an iceberg. This was the first example of a technique in which the environment of catalytic atoms in general could be determined.

The EXAFS technique has been shown to be a powerful tool for studying the arrangement of atoms in multi-component, non-crystalline materials.

Participating Personnel

Farrel W. Lytle, The Boeing Company
Dale E. Sayers, The Boeing Company
Alf K. Eikum, Consultant
Paul A. Franz, Boeing Computer Services

Dr. Sayers received his Ph.D. in Physics from the University of Washington while being supported in part by this contract.

Edward A. Stern and Emmett B. Moore, Jr. collaborated in the research, but were not paid with contract funds.

Contract Publications and Technical Reports

(References)

1. D. E. Sayers, E. A. Stern, F. W. Lytle, "New Technique for Investigating Noncrystalline Structures: Fourier Analysis of the Extended X-ray Absorption Fine Structure," Phys. Rev. Lett. 27, 1204 (1971).

2. D. E. Sayers, F. W. Lytle, E. A. Stern, "Structure Determination of Amorphous Ge, GeO_2, and GeSe by Fourier Analysis of Extended X-ray Absorption Fine Structure", J. NonCryst. Solids 8-10, 401 (1972).

3. D. E. Sayers, "A New Technique to Determine Amorphous Structure Using Extended X-ray Absorption Fine Structure," Ph.D. thesis, Dept. of Physics, Univ. of Washington (1971).

4. F. W. Lytle, D. E. Sayers, A. K. Eikum, "Calorimetric, Diffraction and Microscopic Examination of Evaporated Amorphous Germanium," J. NonCryst. Solids 13, 69 (1973).

5. D. E. Sayers, F. W. Lytle, E. A. Stern, "Determination of Local Structure in Amorphous GeSe, $GeSe_2$, As_2Se_3, As_2S_3 and As_2Te_3 using FXAFS", J. Non-Cryst Solids (to be published).

6. E. A. Stern, D. E. Sayers, "Shielding of Impurities as Measured by Extended X-ray Absorption Fine Structure," Phys. Rev. Lett. 30, 174 (1973).

7. F. W. Lytle, D. E. Sayers, E. B. Moore, "Structure of Catalysts: Determination by EPR and Fourier Analysis of EXAFS," Appl. Phys. Lett. 24, Jan. 15 (1974).

8. F. W. Lytle, D. E. Sayers, "The EXAFS Technique: I. Experiment."

9. D. E. Sayers, F. W. Lytle, E. A. Stern, "The EXAFS Technique: II. Data Analysis".

10. P. A. Franz, D. E. Sayers, F. W. Lytle, "Fast Interactive Computer Graphics for Fourier Transforms of X-ray Data," submitted to J. Appl. Cryst.

The EXAFS Technique: I. Experiment

by

Farrel W. Lytle* and Dale E. Sayers*

The Boeing Company, Seattle, Washington 98124

Abstract

Techniques of x-ray spectroscopy for obtaining extended x-ray absorption fine structure (EXAFS) are discussed. The essential instrumentation is an automated commercial x-ray diffractometer with associated power supply and counting electronics modified to include an improved x-ray monochromator alignment fixture, a cryostat for containing the absorber sample and a card punch for data readout. The preparation of suitable monochromator crystals is discussed. A preset count mode was used to make the most efficient use of experimental time and the technique of multi-pass averaging was used to obtain good counting statistics; i.e. 0.1%. The precision and accuracy of the wavelength/energy scale was determined by replicate analysis and comparison to emission lines from the x-ray source to be ~± leV. When these lines were intense the nonlinear response of the x-ray detecting system required a coincidence correction to be evaluated and applied to the measured counting rates. EXAFS data from Cu is shown as an example.

* Research supported in part by the Advanced Research Projects Agency and monitored by the U. S. Army Research Office, Contract No. DAH C04 71 C 0010.

Introduction

This, and the following paper, describe the experimental details and data processing techniques which we have developed for the practice of x-ray absorption spectroscopy for determination of the structure of non-crystalline solids (For a general treatment of x-ray spectroscopy techniques, see Sandstrom[1].) In our technique the extended x-ray absorption fine structure (EXAFS) is Fourier analyzed to produce a radial distribution function centered on the absorbing atom[2]. The particular utility of the technique is the ability to explore the average environment of each atomic species in multicomponent materials such as amorphous semiconductors[3] or the highly dispersed materials used as catalysts[4]. The basic experimental determinant of the technique is a high resolution, precise measurement of the x-ray absorption coefficient in the neighborhood of characteristic absorption edges. This paper describes the use of a commercial diffractometer (with fairly simple modifications) to produce an x-ray spectrometer of moderate resolution; the diffraction crystals and preparation of the diffractive surfaces; x-ray detectors and counting techniques; and a cryostat and sample transport mechanism.

Summary of theory

During an atomic x-ray absorption event, an x-ray with energy $h\nu$ dissappears and a photoelectron of kinetic energy E is emitted from the atom conserving energy in the process

$$E = h\nu - E_K \qquad (1)$$

where E_K is the initial binding energy of the electron. The absorption follows the law

$$\mu x = \ln I_o/I \text{ or } \ln T/T_o \qquad (2)$$

where μ is the linear absorption coefficient, x is the thickness, I_o is the incident x-ray intensity, I is the transmitted intensity and T and T_o are the times to preset count with the absorber in and out of the beam. On the high energy side of the absorption edge μx shows fluctuations (EXAFS) which are related to the atomic arrangement immediately surrounding the absorbing atom. We have shown that the EXAFS, $\chi(k)$ can be accounted for by a scattering model[5]

$$\chi(k) = \frac{1}{k}\sum_j \frac{N_j}{r_j^2} E(r_j) g_j(2k) \exp(-2\sigma_j^2 k^2) \sin[2kr_j + 2\eta(k)] \qquad (3)$$

where k is the electron wave vector, N_j is the number of atoms in the jth coordination sphere, r_j is the radial distance to the jth atoms, $E(r_j)$ is the scattering potential encountered by the electrons, $g_j(2k)$ is the backward scattering amplitude, the exponential is a Debye-Waller type term where σ_j is the rms fluctuations of the atom about r_j and $\eta(k)$ is a phase shift. The form of this equation makes EXAFS proportional to the number of atoms surrounding the absorbing atom and inversely proportional to r_j^2. A decrease in temperature has its usual effect of sharpening the EXAFS. Each coordination sphere contributes a sine-like term of period $2kr_j$.

Conceptually EXAFS may be visualized as a kind of electron diffraction where the source of the electrons is within the material originating from the atoms of that particular atomic species involved in the absorption event. The mechanism of the absorption fluctuations is as follows: during the dipole transition the electron

oscillates between the initial and final states. Since the final state in this case is located away from the absorbing atom the electron encounters and is scattered by the surrounding potential array. The overlap of the scattered and initial wave functions in the dipole transition matrix produces the EXAFS fluctuations.

X-ray Spectrometer

Our basic x-ray spectrometer (as shown in Fig. 1) is a horizontal diffractometer with attached tube stand. The only modification is an improved crystal (monochromator) support for optimum alignment of the diffracting crystal (Fig. 1b). This spectrometer is used with conventional x-ray diffraction tubes (Ag or Mo target) chosen to provide a high intensity continuum in the region of the absorption edge to be measured. The problem of intense spectral lines which sometimes occur is discussed in the section on counting techniques. We use the spectrometer with a goniometer radius of 18.75 cm and an x-ray tube takeoff angle of approximately 3° (adjusted for maximum diffracted intensity). The first slit is used to limit the angular divergence of the x-ray beam (tube spectrometer mode) and the Bragg-Brentano parafocusing conditions and slit positioning require the focusing (exit) slit to be approximately the same size. The vertical divergence is limited to $\pm 2^{\circ}$ by a Soller slit located before the exit slit. Thus, the resolution function depends primarily on the size of the entrance slit. (See Klug and Alexander[6] for a complete discussion of this type of spectrometer.) Our usual method of operation employs 0.05 mm slits ($.025^{\circ}$ divergence) in the range from 15° to 45° 2Θ and 0.1 mm ($.05^{\circ}$ divergence) slits

Reproduced from best available copy.

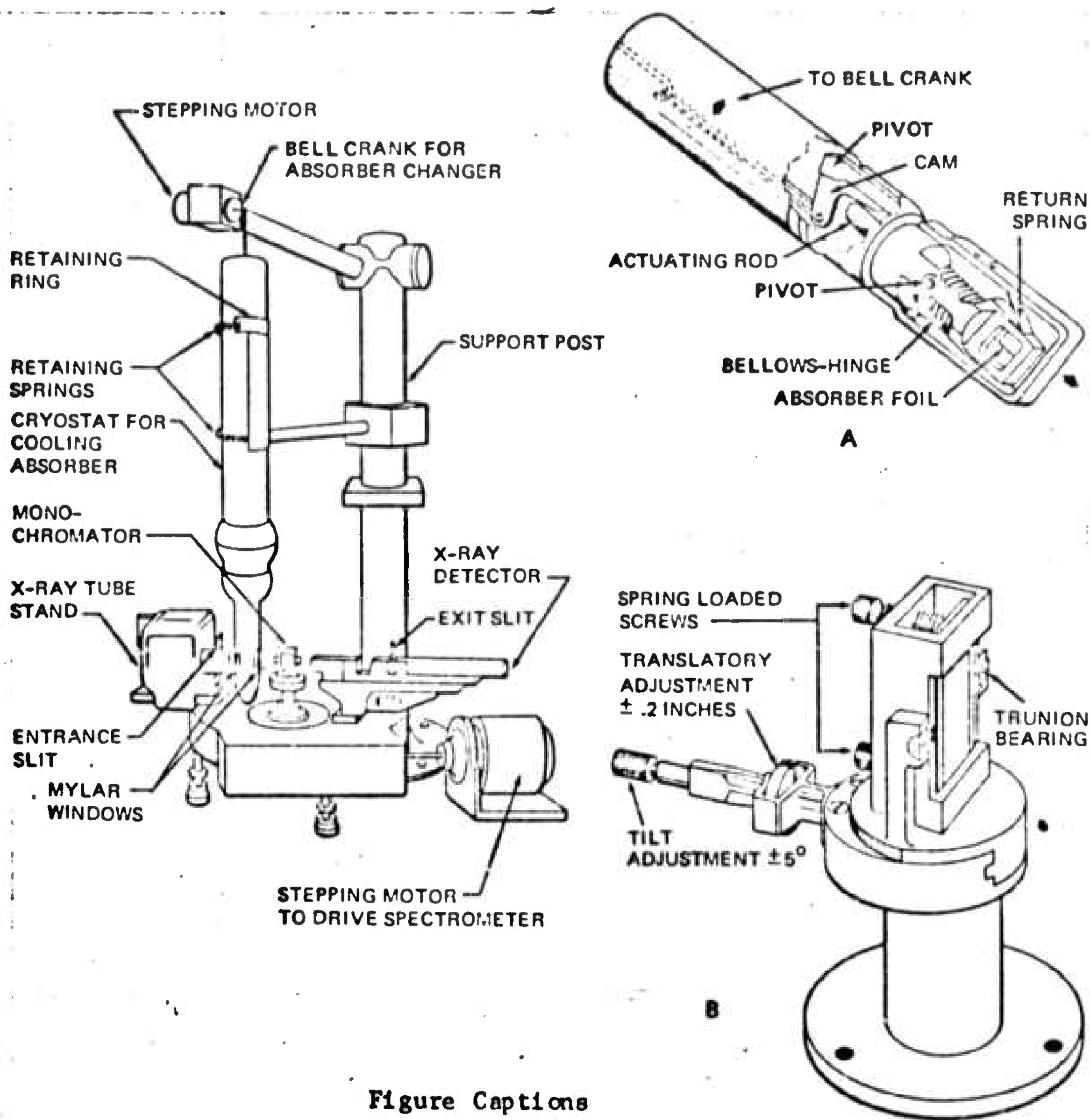

Figure Captions

Figure 1. Sketch of EXAFS apparatus showing the horizontal diffractometer, cryostat, and supporting post.

Figure 1a. The sample holder and movement device. Rotation of the stepping motor bell crank, to which the pull rod is attached, pulls on the rod which actuates the cam and displaces the sample holder using the bellows as a hinge. The spring in the top of the pull rod allows override relief.

Figure 1b. The crystal monochromator support allows translatory motion of the crystal in a direction perpendicular to the incident x-ray beam as well as a tilt adjustment.

for angles greater than 45° with overlap as experimentally required. Hence, the resolving power defined as $\Theta/\Delta\Theta$ is approximately 1500. The diffracted intensity from the continuum operating at full recommended tube KVA depends on wavelength but is typically $1\text{-}10\times10^{3}$ cps.

For the case of 0.05 mm slits at 45° 2Θ and a LiF crystal, the energy band width received at the exit slit would be ~3.5eV. Since the intensity distribution of the radiation filling the exit slit has the usual diffraction profile, the Rayleigh resolution criterion suggests that the spectrometer should be advanced in angular increments of ½ the angular width of the exit slit.

The mode of operation is as follows: For each spectrometer position, T and T_o are measured (preset count) and stored on IBM cards, the spectrometer is advanced to the next 2Θ position and the sequence is repeated. A separate scaler is used to generate a running number for each subsequent pair (T, T_o). Knowledge of the start position and the 2Θ stepping increment allows calculation of the x-ray wavelength for any data pair. The usual experiment involves 500 - 1000 data pairs. The spectrometer stepping motor and absorber changer are activated and synchronized by the x-ray scaler print-out command.

The flanged tube stand attached to the spectrometer allows the x-ray tube to be transtated, rotated, and inclined with respect to the spectrometer circle. The alignment procedure consists of locating (by means of these adjustments) the most intense spot on the x-ray tube target so that it shines through the zeroed entrance and exit slits as measured by a protected x-ray detector. The crystal monochromator is then inserted and a suitable characteristic

line chosen for final crystal adjustment. At the calculated 2θ the translation and rotation (θ) adjustments of the crystal holder are used to obtain peak diffracted intensity of the standard line which locates the diffracting surface of the crystal at the center of the spectrometer. Further refinement of the alignment is not necessary if the procedure described in the section on precision and accuracy of the energy scale is followed.

Cryostat and Absorber

EXAFS has been shown to be sensitive to temperature[7]. The degree of the effect is illustrated in Fig. 2b and 2c which were obtained at 77^oK and 295^oK, respectively. The Debye-Waller type exponential occurring in the theoretical expression for EXAFS can be related to the usual Debye expression[8].

$$\sigma_j^2 = \frac{\hbar^2}{K_B m \theta_D} \phi_j (T/\theta_D) \qquad (4)$$

where θ_D is the Debye characterisitic temperature, σ_j is the rms amplitude of vibration of the atoms in the jth coordination sphere, K_B is Boltzmann constant, m is the mass of the jth atoms, $\hbar$ is Planck's constant/2π, $\phi_j(T/\theta_D)$ is the Debye function, and T is the absolute temperature. Thus, for materials with a low value of θ_D, the temperature effect will be largest, however, all materials will show an EXAFS intensity increase (particularly, far from the absorption edge). For this reason data is obtained routinely at 77^oK (extra sharpness obtained at 4^oK isn't worth the effort). It is possible to use the temperature effect to directly evaluate the shell-to-shell coupling coefficients[8].

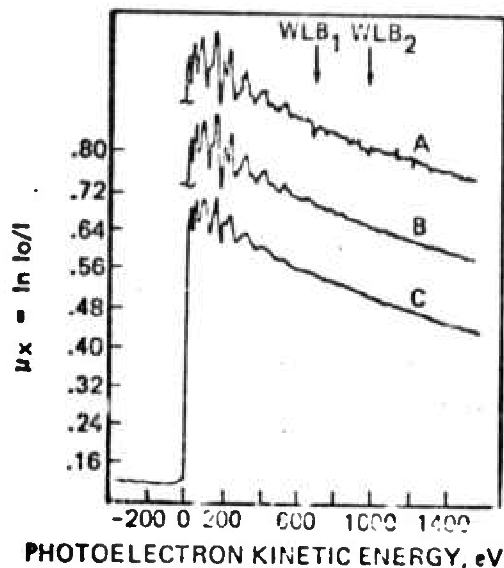

Figure 2. Plots of ln T/T_o vs the energy, E, of the ejected photoelectron for ~ 2.5μm thick Cu foil.

Figure 2a. One pass at 77°K, 10^5 preset count. The features coincident with the W emission lines are due to the nonlinearity of the x-ray detection system. This effect has been removed on the other graphs using a correction technique described in the text.

Figure 2b. Ten passes at 77°K, 10^5 preset count each pass.

Figure 2c. Ten passes at 295°K, 10^5 preset count each pass. Note the smearing of fine structure particularly at high energy.

The glass cryostat illustrated in Fig. 1 contains 5 liters of liquid nitrogen which will last for 3 days. The design of the sample moving mechanism (Fig. 1b) accomplishes its purpose without movable vacuum seals or introduction of a heat leak into the sample area. If a stainless steel bellows is used the fatigue life is 10^6 cycles or 1-2 years of operation. The x-ray transparent windows are 1 mil Mylar expoxied to oval openings in the outer shell.

The absorber samples are prepared in a variety of ways; malleable metals are rolled (2-5μm), some materials may be evaporated onto Mylar or thin Al foil, soluble materials may be dissolved and then absorbed and dried on filter paper, many materials may be ground as fine as possible, mixed with a suitable plastic glue (Duco) and solvent (acetone) then cast on a smooth substrate. When dry, the casts are sandwiched between ½ mil Al for support and thermal contact and attached to the sample holder. The optimum absorber thickness considering contrast, measurement time, and primarily the coincidence counting error problem is attained when $I/I_o \sim 1/3$ on the high absorption side of the edge. The experiments when only a very small amount of the material of interest is present must use thicknesses such that $I/I_o \sim 1/10$. For example with this thickness a satisfactory L_{III} absorption pattern of 0.3 wt % Pt on Al_2O_3 was made in 15 passes.

Monochromator Crystals

The usual discussion of monochromators for x-ray spectrometers emphasizes resolution with narrow crystal rocking curves and multi-crystal spectrometers. Our requirement stresses high x-ray intensity at moderate resolution for good statistical accuracy of measured EXAFS.

Although better resolution would probably show more detail there is an inherent width in the EXAFS due to temperature smearing and uncertainty broadening[9] and a spectrometer with better resolution than the natural width is wasted effort.

The x-ray intensity is limited by the inherent brilliance of the x-ray tube and using flat-crystal optics the count rate is limited by the efficiency of the diffracting crystal and the width of the energy band through the exit slit. The diverging x-rav beam has some distribution in space and energy; i.e. photons/sec/stearadian/eV. The monochromator selects with some diffraction efficiency a band of radiation equal to the angular width of its rocking curve and directs it toward the exit slit. The optimum intensity will occur when the divergence of the incident beam as limited by the first slit and the crystal rocking curve are approximately equal.

The efficiency of diffraction and the rocking curve width of diffraction crystals may be modified by appropriate surface treatment. LiF is a particularly workable crystal in this respect. In Fig. 3 the integrated reflection coefficient, R, for non-polarized radiation which is the area under the crystal rocking curve, has been calculated as a function of wavelength for the two extremes of crystal perfection, a perfect crystal and an ideal mosaic crystal[10]. The measured values of selected cleaved and treated crystals are also shown. Illustrated in Fig. 4 a and b are the full width at half maximum (fwhm) of the rocking curve and the diffraction efficiency ($I_{diffracted}/I_{incident}$) at the peak of the rocking curve. The measurements were made on a double crystal spectrometer in the

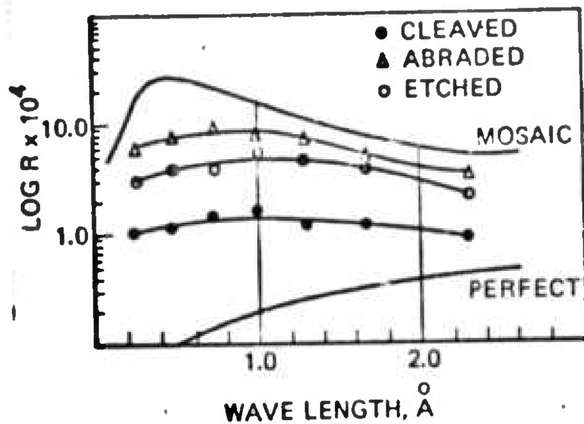

Figure 3. Integrated reflection coefficient vs wavelength for LiF as cleaved, roughened, and chemical polished. The measurements were made on a double-crystal spectrometer correcting for the partial polarization of the incident x-ray beam.

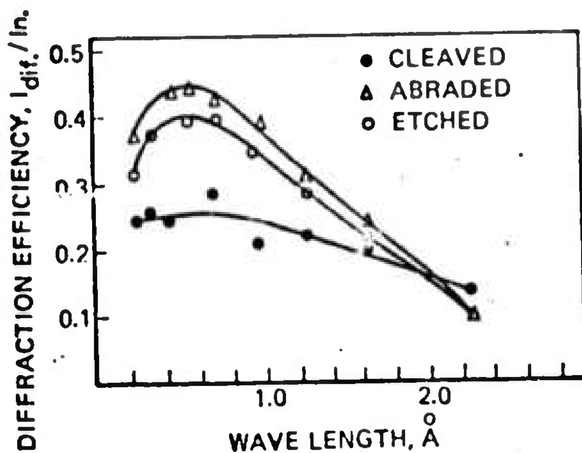

Figure 4b. The intensity ratio, diffracted/incident, at the peak of the diffraction curve for LiF as a function of wavelength and surface treatment.

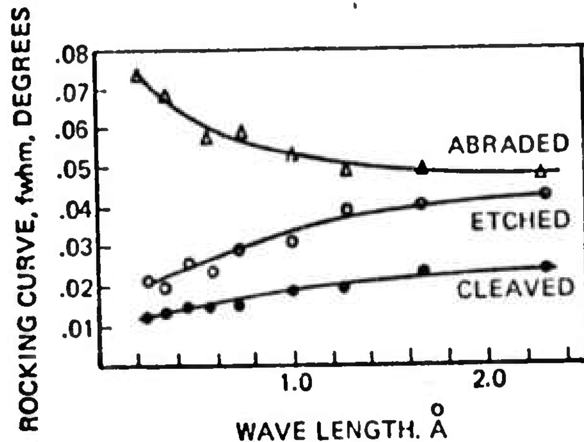

Figure 4a. The full width at half maximum intensity of the rocking curve for LiF crystals as a function of wavelength and surface treatment.

(1, -1) mode using the first crystal to select a monochromatic beam of small angular divergence ($< .01^\circ$). The test crystal was then "rocked" (rotated) through its Bragg angle while the diffracted photons were measured. This is a direct measure[10] of R since

$$R = \frac{\varepsilon w}{I_{in.}} = \int \frac{I_{dif.}}{I_{in.}} d\theta \qquad (5)$$

where ε is the total number of photons counted under the rocking curve, w is the angular rate of crystal rotation (in radians) and $I_{in.}$ and $I_{dif.}$ refer to the incident and diffracted radiation. The measurements have been corrected for the partial polarization of the incident test beam.

These results show that the total radiation diffracted by LiF may be increased by factors of 2-5 by suitable surface treatment to reduce the extinction effects which occur during diffractions[11]. The treatment consists of vigorous sanding on rough paper to drive dislocations into the crystal followed by successively finer paper to 600 grit to provide a smooth surface. This was the treatment of the abraded crystal in Figs. 3 and 4. The damaged surface layer was then removed by an etching procedure[12]. After 1 minute in conc. HF a chemical polish consisting of 2% NH_4OH in H_2O at $26^\circ C$ with vigorous agitation was used to remove the surface at about 1μm/min. The crystal was repeatedly checked until its rocking curve width narrowed to that of the slits. Note that for the etched crystal the diffraction efficiency and R were considerably enhanced over the cleaved crystal. We have used similar techniques with Si and quartz crystals with some success.

Counting Technique

The precision to which the EXAFS function may be determined should be limited by the usual statistics, $\sigma_s = \sqrt{N}$ where σ_s = standard deviation and N = number of photons counted for each data point. This is usually expressed as percent counting error, pce = $(\sigma_s/N) \times 100\%$; e.g. when $N = 10^6$, pce = 0.1%. It would appear that any level of precision could be obtained by making N sufficiently large; but in practice the inherent stability (electrical and mechanical) of the experiment will limit the precision. It is important to determine this value for a particular experiment otherwise time will be wasted by operating at a larger N than warranted.

When the inherent experimental precision has been evaluated (as described below) the experiment is set to accumulate the appropriate number of counts for each data point. If better precision is desired then multi-pass averaging is used to accomplish it.

The inherent precision of our experiment was determined as follows: For a range of N from $10\text{-}10^7$ a subset of data was accumulated for each value of N and σ_s estimated using standard statistics

$$n^{1/2} \sigma_s = \left[\sum_i \left[\left(T_o/T_i \right) - \left(\overline{T_o/T} \right) \right]^2 \right]^{1/2} \quad (6)$$

where T_o and T refer to the time to accumulate N counts, the barred value is the mean of the subset, and n is the number of trials in each subset. The result of this analysis is plotted in Fig. 5 where the difference between the measured and predicted pce; i.e. $\left[\sigma_s(\text{measured}) - N^{1/2} \right] 100/N$ is plotted vs log N. Up to $N = 10^5$

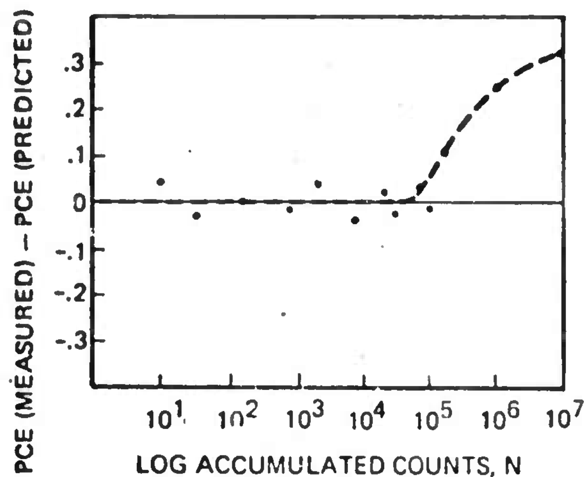

Figure 5. The difference between the predicted and measured percent counting error vs total counts.

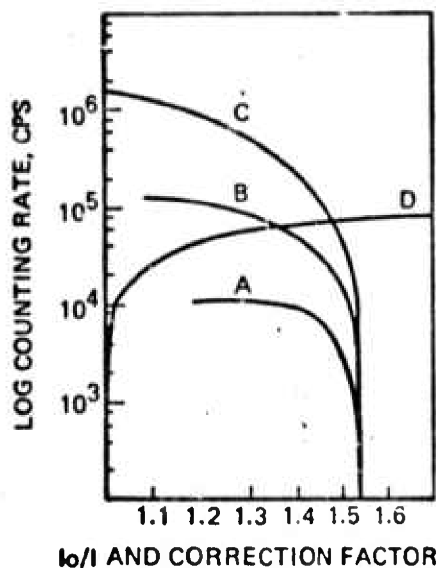

Figure 6. Counting rate vs absorption ratio, I_o/I, for the detecting systems a, b, c described in Table 2. In the region of linear response the ratio is constant, then, since $I_o > I$, I_o decreases relative to I and the absorption ratio decreases. Graph d is a plot of the correction factor (Short's[14] method) for system b which can be multiplied times the measured count rate to correct for nonlinearity.

the data shows a random scatter reflecting the accuracy with which σ_s was measured but at $N = 10^5$ there is a sharp break in the experimental curve indicating that a constant level of precision has been attained no matter how much larger N was made. If the experiment had been completely statistically limited the pce data points would cluster around the zero axis for all N. It is clear from this experiment that accumulating more than 10^5 counts (0.3% pce) is a waste of time. The reason for this fairly high pce was probably due to slight mechanical instability in the cryostat support which allowed the absorber to move in the x-ray beam and reflect irregularities in thickness in the measured signal. The improved precision apparent in the EXAFS of Fig. 2b and 2c was attained by averaging ten separate runs at 10^5 counts for each data point for a final precision near 0.1%.

Precision and Accuracy of the Energy Scale

The kinetic energy of the ejected photoelectrons, E, must be established accurately in order to evaluate the natural EXAFS variable k where

$$k = \left[\frac{2m}{\hbar^2} (E - \Delta W) \right]^{\frac{1}{2}} \qquad (7)$$

where ΔW is the difference between the work function and the average potential seen by the scattered electron. For every experiment characteristic and/or impurity lines from the x-ray tube occur and can be used as standard reference points to establish the energy scale at the accuracy to which they are known[13]. As an example, the lines indicated in Fig. 2 which occurred in the region of the experiment, are tabulated in Table 1. Many elements are present as

Table 1. Precision of Energy Scale

Characteristic Line	Wavelength, Å [13]	Measured 2θ Average of 10 runs	Calculated 2d, Å
W L β_9	1.20479±7	34.838±3	4.02459
W L β_5	1.21545±3	35.162±2	4.02396
W L β_2	1.24460±3	36.026±1	4.02480
W L β_3	1.26269±5	36.564±1	4.02523
W L β_1	1.281809±9	37.142±2	4.02478
W L β_6	1.28989±7	37.387±2	4.02455
W L β_4	1.30162±5	3[illegible] 733±2	4.02524
Cu K β_1	1.392218±9	40.473±2	4.02496
W L η	1.42110±3	41.350±2	4.02502
			Avg. 4.0247±3

impurities on the x-ray tube anode; e.g. W(always present-evaporated from the filament), Cu (always present-evaporated from the anode block), Pb, Ni, Ag, and Zn are usually present, plus the characteristic lines from the primary anode element in multiple orders of diffraction. The presence of these lines always allows a standardization to be made as well as an estimate of the precision with which the energy variable can be established.

As an example the data set for Fig. 2b will be used. Each of ten experimental runs produced an independent value of 2θ for each standard line. The ten values of 2θ were then averaged to obtain one value, listed in Table 1 with the probable error determined from the replicate experiments. Then from Bragg's law and the tabulated values(13), 2d (twice the interplanar spacing) for the monochromator was calculated for each line and a final average obtained. Following this procedure for every set of data removes the requirement for corrections involving the diffraction process such as a temperature correction for the monochromator crystal, Lorentz-polarization correction, refraction and various errors due to misalignment. The final average for the LiF(200) monochromator, 2d = 4.0247 ± 3, is a standard deviation of 75 ppm (typical of our experiments) which would be ± 0.7 eV in the region of the Cu K-edge of Fig. 2. This value of 2d is used in a computer program to calculate (and plot as in Fig. 2) the value of E associated with each data pair (I_o, I) since

$$E = \frac{12398.04}{2d \sin \theta} \text{ eV.} \qquad (8)$$

Note that the error reported for the reference lines (~40 ppm) and the precision to which they can be measured (~50 ppm) are comparable

and are combined in the final determination of 2d(~± 75 ppm). There would be little advantage in a more accurate spectrometer unless a more accurate reference could be established.

Coincidence Losses

In Fig. 2a artifacts appear in the absorption curve at the position of the strong W lines W L β_1 and W L β_2. This effect is due to coincidence losses (nonlinearity) occurring in the x-ray detecting system. Although predictable, these features cause serious errors in EXAFS data analysis. An obvious solution is to use a very fast system with a large dynamic range; however instances will occur where corrections are still necessary.

We have used the components with the performance capabilities described in Table 2.

It is possible to obtain good data with any of these systems provided corrections are made. In the method of Short[14] the absorption of a single absorber is measured as a function of counting rate. When the system becomes nonlinear the measured absorption will decrease since $\mu x = \ln I_o/I$ and I_o, the greater counting rate, will have a proportionally greater nonlinearity. The performance of the three detecting systems is shown in Fig. 6a, b, c. Short's technique can be used to evaluate a correction factor. This factor is plotted in Fig. 6d. We fitted this curve with an equation and during computer processing all data was corrected to remove the effect as in Fig. 2b and c. The correction curve must be evaluated to an accuracy comparable to the data, i.e. 0.1

Table 2. X-ray Detection Systems

Scintillator	Preamplifier-Amplifier - PHA*	Scaler
a. NaI with Siemens phototube	Old Siemens tube type, rated 2 Kilohertz	Siemens tube type
b. NaI with XP 1010 phototube	Hamner solid state, rated 100 Kilohertz	Hamner solid state, rated 10 Megahertz
c. 5% Sn-filled organic with PM 2106 phototube	Close-coupled IC video pre amp. measured 45 Megahertz. EC&G logic type amp/discrim. measured 50 Megahertz	Cambridge, rated 10 Megahertz with EG & G scale of 8 pre scaler

Notes: NaI, 250ns decay time.
5% Sn-filled organic, 2ns decay time.
XP 1010, 4ns risetime.
PM 2106, 1.3ns risetime.

* PHA - pulse height analyzer

Discussion

The experimental requirements of the EXAFS technique are within range of anyone who can dedicate a commercial x-ray diffractometer, power supply, and counting rack to this use. The necessity for multi-pass averaging to obtain good statistics for the most difficult (and most interesting) absorbers requires a full-time operation with approximately 24 hours for each pass through the EXAFS region. Since the experiment is easily automated this is not a handicap. Indeed, our experiments are turned off only for maintenance every few months.

The additional equipment items which are essential are 1) the improved diffraction crystal holder. (The intensity gained by optimizing alignment through narrow slits can be a factor of 10.) 2) The cryostat and sample movement device. 3) A card punch for data readout. Other methods, such as paper tape or magnetic tape, lack the advantage of immediate visibility and easy correction of occasional erroneous data points.

After the data is acquired and the multipass average is obtained the very considerable problem of data analysis remains which is the subject of the following paper.

References

1. A. E. Sandstrom in Handbuch der Physik Vol. 30, p. 78 (Springer Verlag, Berlin, 1957).

2. D. E. Sayers, E. A. Stern, F. W. Lytle, Phys. Rev. Lett. 27, 1204 (1971).

3. D. E. Sayers, F. W. Lytle, E. A. Stern, J. Non-Cryst. Solids 8-10, 401 (1972).

4. F. W. Lytle, D. E. Sayers, E. B. Moore, Appl. Phys. Lett. 24, 1974.

5. D. E. Sayers, F. W. Lytle, E. A. Stern, in "Advances in X-ray Analysis", Vol. 13, p. 248 (Plenum, New York, 1970).

6. H. P. Klug, L. E. Alexander, "X-ray Diffraction Procedures", p. 235 (John Wiley, New York, 1954).

7. J. D. Hanawalt, Z. Physik 70, 293 (1931); J. Franklin Institute 214, 569 (1932): F. W. Lytle, in "Dev. in Applied Spectroscopy" p. 285 (Plenum, New York, 1963).

8. V. V. Shmidt, Bull. Acad. Sci. USSR, Ser. Phys. 25, 988 (1961); 27, 392 (1963).

9. L. G. Parratt, Rev. Mod. Phys. 31, 616 (1959(

10. R. W. James, "The Optical Principles of the Diffraction of X-rays" p. 268 (G. Bell, London, 1958).

11. J. Vierling, J. V. Gilfrich, L. S. Birks, Applied Spectroscopy 23, 342 (1969): F. W. Lytle, Science 165, 416 (1969).

12. J. J. Gilman and R. Johnston, "Dislocations and Mechanical Properties of Crystals", p. 119 (John Wiley, New York, 1957).

13. J. A. Bearden, Rev. Mod. Phys. 39:1, 78 (1967).

14. M. A. Short, Rev. Sci. Instr. 31, 618 (1960).

The EXAFS Technique: II Data Analysis

by

Dale E. Sayers* and Edward A. Stern†
The University of Washington, Seattle, Washington 98105
and
Farrel W. Lytle*, The Boeing Company, Seattle, Washington 98124

Abstract

The technique of computer processing of extended x-ray absorption fine structure (EXAFS) for the analysis of non-crystalline solids is discussed. The topics include: normalization of the data to a per atom scale, Fourier filtering to remove the sloping background, and a Fourier transform of the data into a radial structure function. Particular factors peculiar to EXAFS are emphasized; e.g. upper and lower limits of integration, the effect of the phase shift on the determination of interatomic distances, the peak shape and the determination of coordination numbers. The EXAFS spectrum of crystalline Ge is used as an example.

* Research supported in part by the Advanced Research Projects Agency and monitored by the U. S. Army Research Office, Contract No. DAH C04 71 C 0010.

† Research supported in part by the U. S. Air Force Office of Scientific Research.

Introduction

The previous paper described the experimental requirements for obtaining EXAFS data.[1] This paper discusses the processing and analysis of EXAFS data concentrating on the important factors which are specifically related to EXAFS. The analysis and discussion are limited to K-shell absorption spectra only. The techniques and information involved in L-shell spectra will be published elsewhere.[2] The general subject of finite Fourier transforms has been much discussed by others involved in x-ray radial distribution analysis.[3] This paper emphasizes the processing of the raw data, the removal of the EXAFS from the average absorption background using a Fourier filtering technique, and the normalization of the EXAFS according to the theoretical expression so that all data are on the same per atom scale. Fourier transformation using the point-scattering theory results in a radial structure function centered on the absorbing atom. This feature permits evaluation of unique correlation functions for each atomic species in a multi-component material and is the major achievement of the EXAFS technique. The particular problems of changing from an energy to a wave vector scale, selecting the upper and lower limits of integration, the phase shift, and the peak shapes are discussed in detail.

Initial Data Processing

The data collected from our EXAFS apparatus consists of the time to collect a preset number of counts (usually 10^5) with the absorber in and out of the beam, respectively (T, T_o) along with the corresponding step number at each angular position of the spectrometer. A typical data deck consists of approximately 200-300 cards with 4 sets of T, T_o and the running number per card. The preliminary data processing program (1) tabulates the initial data and calculates the x-ray energy, the kinetic energy of the photoelectron, and the total absorption; (2) removes the oscillatory part of the x-ray absorption from the smooth monotonic background; and (3) normalizes the data to a per atom scale. These three program functions are described below.

In addition to tabulating the input data the program routinely calculates the absorption and energy scales from input data. Specifically, the total absorption is calculated at each point using

$$\mu x = \ln(T/T_o) \tag{1}$$

as described in the previous paper.[1] The x-ray energy at each point is found from

$$h\nu = \frac{12398.04}{2d \sin\theta} \tag{2}$$

where (2d) is calculated as described previously[1] and θ at each spectrometer setting is found from the initial angle and fixed angular step. The kinetic energy of the ejected photoelectron is then

$$E = h\nu - E_K \tag{3}$$

where E_K is the initial binding energy of the 1s electron which was ejected during the absorption of the x-ray. The tabulated binding energies of Bearden and Burr were used.[6]

The next step in the processing involves removing the K shell contribution for the atomic species of interest from all other absorption components including other shells in the same atom, absorption by other atoms in the sample, and absorption by the specimen support which is usually Al foil. In the energy region of interest these other components are usually far from any characteristic edges and may be adequately described by a Victoreen formula[7] of the form $\mu = C\lambda^3 + D\lambda^4$ where λ is the x-ray wavelength and C and D are found by fitting this formula to the measured absorption curve over an energy range (typically a few hundred eV) just below the K-edge of interest. This fitted curve is then extrapolated to energies above the absorption edge to approximate all of the other absorption components and is subtracted from the experimental curve. The remainder is the K shell contribution to the absorption including the EXAFS ($\mu_K(k)$).

The removal of the oscillatory part of the x-ray absorption coefficient (EXAFS) from the smooth, monotonically-decreasing background absorption is a difficult problem since neither calculated nor empirical curves exist which are accurate in the vicinity of the absorption edge. Rather than fitting some empirical function far above the edge and extrapolating back to the edge where large uncertainties may occur we have chosen to use a Fourier filtering technique. This technique uses a fast Fourier transform algorithm on the raw data (which is equispaced in θ) and takes 2048 data points and analyzes them in terms of the real and imaginary components of 1024 frequencies. The lowest frequency has a wavelength of twice the range of the data and the remaining frequencies are the next 1023 harmonics of this fundamental. This spectrum has 3 components: (1) contributions at low frequencies due to the monotonically decreasing absorption coefficient; (2) the EXAFS signal at intermediate frequencies; and (3) small components from the random statistical counting noise uniformly distributed throughout the entire frequency range. The lowest EXAFS frequencies were estimated on the basis of the typical near neighbor distances and were well separated from the low frequency components which could then be filtered by zeroing the first few low frequencies and retransforming the spectrum. This is shown in Figure 1 where 70 of the first 512 coefficients of a typical transform are shown. The remaining coefficients are negligible. The arrow indicates where a typical cut would be made to filter out the monotonic background. This transformed spectrum contains only contributions from EXAFS and the noise. The smooth absorption background may be found by subtracting this filtered spectrum from the raw data.

The entire normalization procedure is shown in Figure 2. Figure 2(a) shows the Ge K-edge EXAFS for amorphous GeSe along with the extrapolated Victoreen curve (dashed line) which was fitted to the data in the energy region below the edge. In Figure 2(b) the EXAFS which was obtained from the data in Figure 2(a) using the Fourier filtering technique is shown and in Figure 2(c) the smooth background curve obtained by subtracting the curve in Figure 2(b) from the curve in Figure 2(a) is also shown. Figure 2(c) also compares this smooth background curve $\mu^o_K(k)$ to both a Victoreen formula[7] and the empirical $\lambda^{2.73}$ curve suggested by

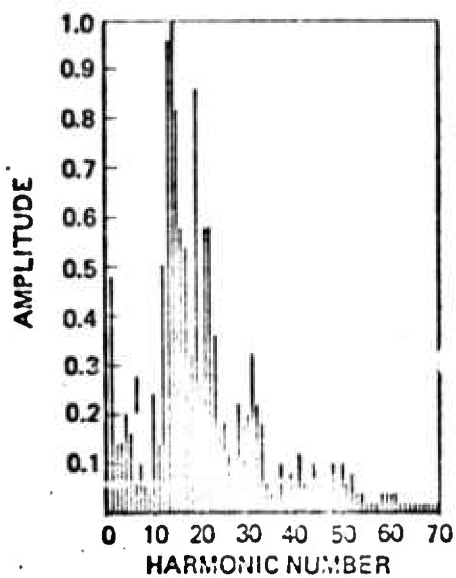

Figure 1. Example of a frequency spectrum of the raw data using a fast Fourier transform. The separation of EXAFS from the low frequency slope components is apparent. The arrow indicates where the low frequency cutoff is made. Only 70 of the 512 components are shown; all higher components are negligible.

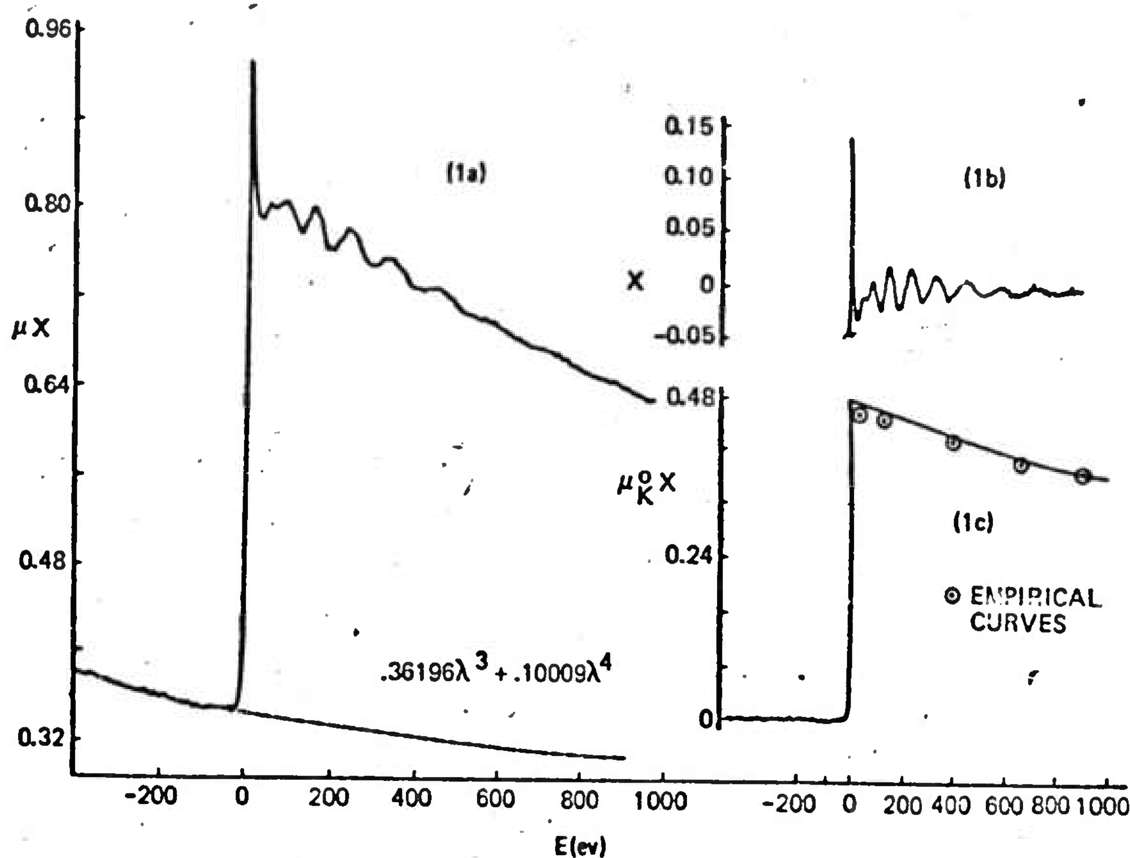

Figure 2a. The measured K-edge of Ge in amorphous GeSe where μx (absorption coef. times thickness) is plotted vs the photoelectron kinetic energy, E. The dashed line is the Victoreen formula extrapolation due to absorption from other than the Ge K-shell.

Figure 2b. χ vs E normalized and extracted from Figure 2a as explained in the text.

Figure 2c. The smooth K-shell absorption background $\mu_K(x)$ vs E which was used to normalize χ according to equation (4). $\mu_K(x)$ is obtained from Figure 2a by subtracting the Victoreen extrapolation (dashed line) and Fourier filtering to remove the EXAFS. The points Θ are extrapolations to the edge from a region 1000-1500 eV above the edge of both a Victoreen form and the empirical formula of McMaster.[8] Both are identical and approximately 5% below the measured curve.

McMaster[8]. These curves were normalized to the data in the region 1000-1500 eV above the edge and give essentially identical results. As can be seen the fit is good to 500-1000 eV but is lower than the data curve by ∿5% near the edge, which would give noticeable curvature to the EXAFS (Figure 2(b) if they had been used. We have also checked the sensitivity of this technique to the number of components which were zeroed, and have found no significant deviation from the smooth curve as long as the number of components zeroed was less than the expected minimum EXAFS frequency (i.e. if no more than the first 10 frequencies are zeroed).

The final step in the initial data processing involves normalizing the data according to the definition

$$\chi(k) = \left[\mu_K(k)/\mu_K^o(k)\right] - 1 \qquad (4)$$

where $\chi(k)$ is the EXAFS, $\mu_K(k)$ is the total K-shell contribution to the x-ray absorption coefficient and $\mu_K^o(k)$ is the smooth monotonically decreasing background of the K shell. The EXAFS defined in this way normalizes all data to the same per atom scale which will allow absolute coordination numbers to be determined (as described below). $\mu_K(k)$ and $\mu_K{}^o(k)$ are determined as described above and the normalized EXAFS $\chi(k)$ is determined using these functions and equation (4). The data analysis program plots μx vs. E and χ vs. E and punches a deck of χ,E pairs which is used as the input for the final data analysis.

Fourier Analysis of EXAFS

Fourier analysis of the normalized data is based on the point-scattering theory of EXAFS for K-shell absorption[4,5,9]

$$\chi(k) = 1/k \sum_j \frac{N_j}{r_j^2} E(r_j)\, g_j(2\vec{k}) \exp(-2\sigma_j^2 k^2) \sin\left[2kr_j + 2\eta(k)\right] \qquad (5)$$

Here $g_j(2\vec{k})$ is the backward-scattering amplitude from the surrounding atoms in the jth shell of the excited p-state electron of wave number k per unit electric field. The direction of $\vec{k}$ is radially out from the excited atom to the center of an atom in the jth atomic shell; $E(r_j)$ is the average electric field induced at r_j(the position of the jth shell of atoms) by

the ionized atom at $r = 0$. N_j is the total number of atoms in the jth shell and σ_j^2 is a measure of the fluctuations of the actual positions of the atoms in the jth shell about their average position r_j. The exponential containing σ_j^2 is a Debye-Waller-type factor.

Since EXAFS can be viewed as a sum of damped sine waves we can formally invert the data using Fourier analysis. In most monatomic materials we find that $g(2\vec{k})$ is independent of r_j to a good approximation so that equation (5) can be rearranged and transformed with respect to $\sin(2kr+2\eta(k))$ to give

$$\phi(r) = \frac{1}{\sqrt{2\pi}} \int_0^\infty \frac{k\chi(k)}{g(2k)} \sin(2kr+2\eta(k)) \tag{6a}$$

$$= \frac{N_j E(r_j)}{8r_j^2\sigma_j} \exp(-(r-r_j)^2/2\sigma_j^2) + \Delta r \tag{6b}$$

where equation (6b) is obtained from equation (6a) using equation (5), and $\phi(r)$ is a radial structure function which gives the location of atoms around the absorbing atom in terms of a series of gaussian-shaped peaks whose amplitudes are proportional to N_j. Δr contains a symmetrical exponential term which is not used and other terms much smaller than $\phi(r)$.

While the integration of equation (6) is illustrative to show the kinds of information available from EXAFS it ignores several factors which must be accounted for in the actual data analysis including the finite upper and lower limits of integration, the fact that $g(2k)$ and $\eta(k)$ are not, in general, known and that the definition of k is uncertain. Specifically the integral that is actually calculated is

$$\phi(r) = \sqrt{\frac{1}{2\pi}} \int_{k_{min}}^{k_{max}} \chi(k) \exp(2ikr)dk \tag{7}$$

The problems involved in equation (7) fall in 2 categories (evaluation and interpretation) and will be discussed separately.

A) Evaluation - The photoelectron wavevector is evaluated from the definition

$$\frac{\hbar^2 k^2}{2m} = E - (U_o - W) \tag{8}$$

where E is defined by equation (3) and is referenced to the Fermi energy, U_o is the average inner potential measured from the vacuum level and W is the work function. For metals U_o-W is on the order of the Fermi energy measured from the bottom of the conduction band. In semiconductors and insulators the zero of kinetic energy is not as easy to define but may be approximated by averaging the pseudo-potential over the energy range of interest. In either case errors, ΔE, of a few eV may arise in the choice of U_o-W used. These errors do not significantly affect the data since even at the energy corresponding to the lower limit of integration (typically $E_L \sim 50$eV), $\Delta E/E_L$ is negligible. We have verified this on several spectra by varying U_o-W over a suitable range and found no significant effects on the transforms.

Another problem in evaluation is the choice of upper and lower limits of integration in equation (7). The upper limit is determined primarily by the experimental range of energies which have been measured, typically, 1000-1500 eV above the edge (which corresponds to a k range up to 15-20 Å^{-1}) unless other absorption edges appear in the data. It is usually desirable to have k as large as possible to reduce the termination error found in Fourier transforms which are truncated[3] at finite k, although these effects are not the primary cause of deviations from the gaussian-peak shape predicted by equation (6b) as will be discussed below. The lower limit of integration is generally determined by the requirement that it is far enough above the edge so that the assumptions of the point scattering theory are valid and any band structure effects on the density of states have disappeared. There is no precise point at which this occurs but is typically $\sim$30-50 eV and may be verified by choosing several lower limits and selecting the one which produces the cleanest transform (i.e., low noise at $r<1\text{Å}$).

The actual transform may be done either by direct integration or by using a Fast-Fourier algorithm. In order to process large amounts of data with the capability to make real time decisions we have developed a program using a display scope with interactive capability[10]. The outputs are the real (cosine), imaginary (sine), and magnitude of the transform. In Figure 3 the EXAFS for crystalline Ge over the range to be transformed is shown. In Figure 4 the transform of the data from Figure 3 is shown over the range of k from 4.1 to 15.8$\mathring{A}^{-1}$, where 4(a) is the real part, 4(b) the imaginary part, and 4(c) is the magnitude of the transform. As can be seen the imaginary and magnitude have several peaks which contain structural information. The factors which affect the interpretation of these transforms and the information contained in the transform is discussed in the next section.

B) Interpretation - There are several qualitative features which help understand the data. First, as can be seen in Figure 4, there is very little amplitude in the region below 1$\mathring{A}$. This condition can usually be achieved by proper selection of the lower limit of integration and indicates that there are no large normalization or background subtraction errors which have been known to affect the transforms strongly in this region[11,12]. Because of the uncertainties which have been discussed in removing the EXAFS from the background absorption it is likely that some error has been introduced in the transform; however, our experience is that these errors can be made small.

The relationship between the real part, imaginary part and magnitude of the transform is apparent in the first large peak in the data (between 1-3$\mathring{A}$). If the theoretical expression from equation 5 is inserted into equation 7 and it is assumed that $\eta=0$ and the k dependence of the factor g $(2\vec{k})/k$ is neglected the result would be a symmetric gaussian-shaped imaginary part and an antisymmetric real part centered on the shell distance, r_j. This is what is observed in Ge for the first shell. The peak shape of the imaginary part has deep negative side lobes, which will be discussed later, but this does not change the basic relationship between the two parts of the transform. In fact, the two parts of the transform contain complementary information so that only

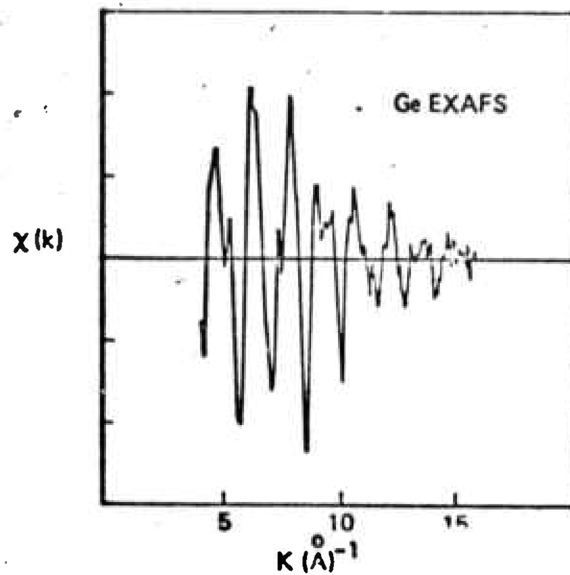

Figure 3. $\chi(k)$ vs k ($\mathring{A}^{-1}$) for crystalline Ge. Data is shown only in the region 4.1 - 15.8 $\mathring{A}^{-1}$ which is Fourier transformed in Figure 4.

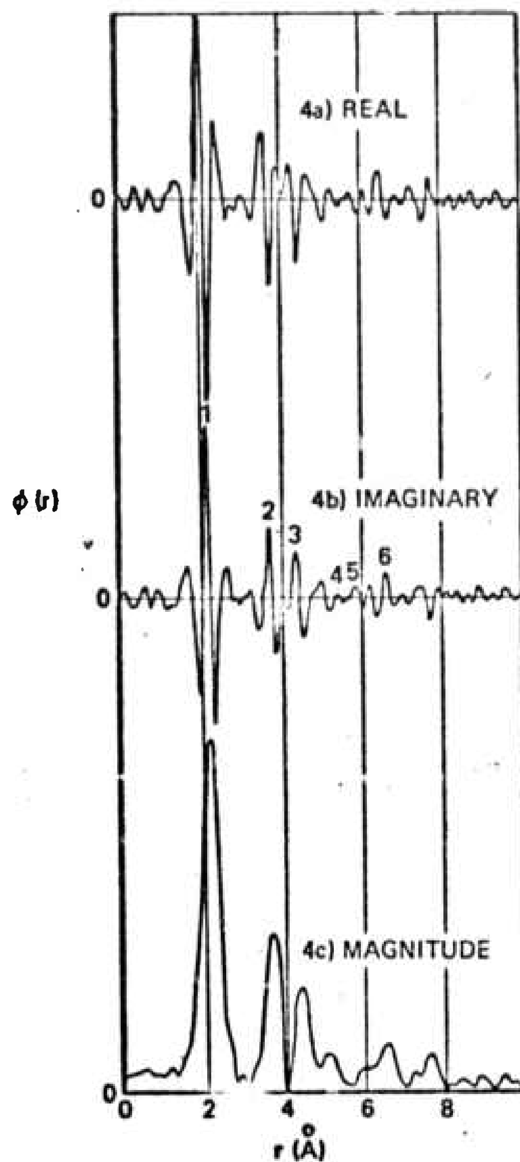

Figure 4a, 4b, 4c. The real part, imaginary part, and magnitude, respectively, of the Fourier transform of the EXAFS in Figure 3 plotted $\phi(r)$ vs $r(\AA)$. The numbers over the peaks locate the first 6 coordination shells. The $\phi(r)$ scale in 4c is twice that of 4a and 4b.

one part need be studied. The situation is somewhat complicated by the finite constant phase shift. By using simple trigonometric identities it can be shown that the real and imaginary parts now are admixtures of the $\eta=0$ transforms so that neither part is completely symmetric or antisymmetric unless the phase is a multiple of $\pi/2$. Location of the peak position may still be made using the magnitude of the transform which is independent of any constant phase shift and will be peaked at $r=r_j$. In the case of Ge it appears that the constant part of the phase is approximately zero since the real and imaginary parts of the Fourier transform have the shapes described above. Note that the magnitude (Figure 4c) is peaked at the same place as the imaginary (Figure 4-) part but is smoother and broader which in some ways makes it easier to identify shell locations since it reduces the effects of the side lobes.

To locate the peak position accurately it is necessary to understand the phase shift more fully. Estimates of the phase shifts using the WKB[13,14,5] method have shown that for most elements the phase shift is approximately linear in k over the EXAFS energy range with a negative slope, i.e.

$$\eta(k) = -\alpha k+\beta \tag{9}$$

with α,β constant. This linearity has been verified in the case of Cu using a more exact calculation of phase shifts using a Hartree-Fock potential.[15] Substituting equation (9) into equation (5) gives the argument for the sine wave of $(2kr-2\alpha k+2\beta)$. The effect of the constant phase 2β has been discussed above; however, as first pointed out by Mott[14], the linear k dependent term shifts the "frequency" of the sine wave from r_j to $r_j-\alpha$. In the Fourier transform this has the effect of shifting all peaks toward the origin by an amount α. In crystalline materials where the distances, r_j, are known the transforms may be used to evaluate α. This is shown in Table I where the data for the transforms shown in Figure 4 is tabulated. Column five of the table shows that for the first 3 shells where the data is most reliable a value of $\alpha = .28\mathring{A}$ may be used.

Table I. EXAFS Structural Data For Ge

j	N_j	$r_j(\mathring{A})$	$r_j'(\mathring{A})$	$\alpha(\mathring{A})$	A_j/A_1
1	4	2.45	2.17	.28	1
2	12	4.00	3.72	.28	.45
3	12	4.68	4.41	.27	.30
4	6	5.65	5.38	.27	.04
5	12	6.16	5.83	.33	.06
6	24	6.92	6.60	.32	.13

r_j = known jth shell distance for dia. cub. Ge ($d=5.65\mathring{A}$)

r_j = measured peak position from Figure 4b

$\alpha = r_j - r_j'$

A_j/A_1 = amplitude of the imaginary transform at r_j' normalized to the first shell amplitude

This data also shows at least 6 shells in Ge may be located although there are other features in the data at $\sim 5\mathring{A}$ and $\sim 6.2\mathring{A}$ which can't be explained by the simple point scattering model. The value of α which can be determined from known structures is typically accurate to $\pm .02\mathring{A}$ which gives a total accuracy of 2-3% in the distance measurements. To determine distances in materials where the crystal structure is not known (such as amorphous materials or biological systems) assumptions must be made about the phase shift. Generally, the phase shift is dominated by the potential well created by the inner vacancy in absorbing atom itself and not by its surroundings so that all Ge atoms should have approximately the same phase shift regardless of the compound it is in. This is verified by the data in Table II where the k dependence of the phase shifts in a variety of materials whose structures are known are listed. The Ge phase shifts in the Ge compounds agree very well with the value of $\alpha = .28$ determined from crystalline Ge. The values of α for several other elements in the third row of the periodic table are listed and show that α is between .25 and .41 in this region of the periodic table. To minimize the uncertainties in assigning α for unknown structures we have used standard compounds whose composition and local structure are known and whose local environment is expected to be similar to the local structure being investigated. As a general rule we have found that compounds among atoms in the same row of the periodic table (especially if the valence of the absorbing atom is small) tend to have phase shifts similar to the pure element whose edge is being studied. We have also found that in some systems, particularly certain oxides with ionic bond, there are significant deviations from the elemental phase shifts. Further experimental and theoretical studies are underway in order to quantitatively understand the observed phase shifts and their origins and make reliable structural measurements in a wider variety of systems.

As mentioned above the shapes of the peak differ significantly from the gaussian shape predicted by equation (6b) even if termination effects are taken into account. This is because in the actual transform (equation (7)) the k dependence of the factor $g(2k)/k$ has not been removed from the data so that the experimental transform is a convolution of the

Table II. Phase Shift k Dependence (α from equation 9) for Several Elements and Compounds

Material	α	Material	α
Cr	.36	Ge	.28
Fe	.26	Se	.26
Ni	.25	$(Ge)O_2$	.27
Cu	.38	$(Ge)Se_2$	.29
Zn	.41	(Ge)Se	.29
As	.27		

result of equation (6b) with the Fourier transform of $g(2k)/k$. The general shape of this function is the envelope of the EXAFS shown in Figure 3 which, for many systems, increases to a peak about $k = 6\text{-}7\ \mathring{A}^{-1}$ and decreases at higher k. This envelope also includes temperature effects but these decrease monotonically with k and do not give the peaking which is observed. The transforms of a variety of similar envelope functions have been studied by Waser and Schomaker[17] who show that the results are transforms with large negative side lobes as observed in Figure 4. At present the functional form of $g(2k)$ is not known well enough to separate its effect from the data. This complicates the analysis particularly at large r where the shells are close enough together so that the side lobes interfere with adjacent peaks making peak identification uncertain. The peak shape also makes interpretation of the amplitude difficult. From equation (6b) the amplitude of each peak is proportional to $N_j E(r_j)/\sigma_j r_j^2$, and by a standard integration the area under the peak is proportional to $N_j E(r_j)/r_j^2$. However, the area is difficult to measure accurately so the amplitude is usually used to obtain any information about number of atoms per shell. Since r_j is determined from the peak location, the amplitude contains information proportional to $N_j E(r_j)/\sigma_j$. When the data is normalized according to equation 4, all data are on the same scale and could be compared directly to determine the coordination numbers, N_j, if $E(r_j)/\sigma j$ were known. Normally, this is not the case so reliable coordination numbers are obtained by empirical comparisons. In some crystalline systems σ_j may be calculated and the measured amplitude used with the known crystal structure to determine $E(r_j)$; however, it is usually not possible to measure enough amplitudes reliably to differentiate between possible forms for $E(r_j)$ (e.g. power law vs. exponentail). It is also possible to measure the temperature dependence of the amplitudes to determine σ_j experimentally. In multi-component materials where only one absorption edge can be measured,[17] we have assumed that $E(r_j)$ is primarily a function of local environment and used standard compounds whose environment and coordination are expected to be similar to the unknown system to determine N_j. We estimate that this procedure can give coordination numbers which are good to $\sim$20% for the first few shells.

Recently, we have extended this procedure to making absolute measurements of the first neighbor coordination of both species in binary compounds where each atom's EXAFS can be measured.[18] It was possible to determine the number of each kind of first neighbor atom around both species. This technique was limited to systems for which good standards could be used for a reference, but did give reliable results for amorphous $GeSe_2$ and As_2Se_3 which are similar to their crystalline polymorphs. To obtain more reliable coordination numbers will require a better understanding of the meachanisms which determine E(r) and g(2k), so that these factors can be determined reliably without the use of standard compounds.

Discussion

The Fourier transform of EXAFS data can be used to determine the local atomic environment of each kind of atom in multi-component non-crystalline materials. It is a general and powerful tool for studying any physical state of matter, solid, liquid, or gas. It has been applied to amorphous semiconductors,[5,9,18] supported catalysts[17] and biological materials (yet to be published).

The data processing is concerned with extraction of the EXAFS from data containing the effects of other physical processes in a form suitable for Fourier analysis, which is a difficulty common to other scattering methods.[3] However, there are particular factors peculiar to EXAFS such as the phase shift, definition of the wave vector scale, and an unknown scattering factor which are the primary concerns of this paper. We have addressed these problems in a completely pragmatic way by using well-matched standard materials to determine these parameters and then applying them to the unknown materials. As such, the technique is useful for studying the atomic arrangement in non-crystalline materials but suffers a lack of completeness. As more materials are studied and the parameters become more accurately defined, we trust that theory will catch up. In addition to the structural information emphasized here, the x-ray absorption edges contain a wealth of physics which is becoming apparent as we have tried to understand the EXAFS technique; e.g. some L-spectra show giant resonances at the edge with s-d mixing in the EXAFS[2] and the role of impurity-charge shielding in EXAFS has been discussed.[9]

References

1. F. W. Lytle, D. E. Sayers, preceding paper.

2. F. W. Lytle, D. E. Sayers, E. A. Stern, P. A. Lee, to be published.

3. B. E. Warren, "X-ray Diffraction" (Addison-Wesley, 1964).

4. D. E. Sayers, F. W. Lytle, E. A. Stern in Advances in X-ray Analysis, B. L. Henke, J. B. Newkirk, G. R. Mallett, ed (Plenum, 1970), Vol. 13, p. 248.

5. D. E. Sayers, Ph.D Thesis, University of Washington, 1971 (unpublished).

6. J. A. Bearden, A. F. Burr, Rev. Mod. Phys. 39.1, 78 (1967).

7. International Tables for X-ray Crystallography III, K. Lonsdale et. al ed. (Kynoch, 1962) Sec. 3.2.

8. K. F. J. Heinrich, "The Electron Microprobe," McKinley, Heinrich, Wittry (ed.) (Wiley, 1966) p. 296.

9. D. E. Sayers, E. A. Stern, F. W. Lytle, Phys. Rev. Lett. 27, 1204 (1971), E. A. Stern, D. E. Sayers, Phys. Rev. Lett., 30, 174 (1973).

10. P. A. Franz, F. W. Lytle, D. E. Sayers, J. Appl. Cryst., submitted.

11. A. Bienenstock, J. Chem. Phys. 31, 570 (1959).

12. R. Kaplow, S. L. Strong, B. L. Auerbach, Phys. Rev. 138:5A, A1136 (1965).

13. A. T. Kozlenkov, Bull. Acad Sci. USSR, Ser.Phys. 25, 968 (1961).

14. D. L. Mott, Ph.D. Thesis, New Mexico State University, unpublished, (1963).

15. P. A. Lee, private communication.

16. J. Waser, V. Schomaker, Rev. Mod. Phys., 25, 671 (1953).

17. F. W. Lytle, D. E. Sayers, E. B. Moore, Appl. Phys. Lett. 24, Jan. 15 (1974).

18. D. E. Sayers, F. W. Lytle, E. A. Stern, Proceedings of the 5th International Conference on Amorphous and Liquid Semiconductors (to be published in J. Non-Cryst. Solids).

*FAST, INTERACTIVE, COMPUTER GRAPHICS
FOR
FOURIER TRANSFORMS OF X-RAY DATA

BY

Paul A. Franz
Boeing Computer Services, Inc.

Dale E. Sayers
The Boeing Aerospace Company

Farrel W. Lytle
The Boeing Aerospace Company

November, 1973
Seattle, Washington 98124

B

ABSTRACT

A computer program is described which allows real-time data analysis decisions by means of a display scope for Fourier transforms, data manipulation, and inverse transforms of x-ray data. The example given analyzes the Ge K-edge extended x-ray absorption fine structure; however, any x-ray, electron, or neutron scattering data could be analyzed.

INTRODUCTION

Fourier transforms of experimental data are widely used in many areas of physics including x-ray and electron scattering and extended x-ray absorption fine structure (EXAFS) experiments as well as many other applications. Often these transforms involve large amounts of data and are very time-consuming; however, the development of the Fast Fourier Transform (FFT) algorithm (Cooley & Tukey, 1965) resulted in substantial time savings. Data analysis may still be time-consuming, particularly if real-time decisions must be made regarding optimum termination points, multiplication by termination functions, inverse transforms, and display of final data, which traditionally means several individual computer runs with resultant turnaround time.

These shortcomings have been overcome with the development of a data analysis program which uses a vector display scope on line with a large digital computer. This interactive computer program allows rapid initial processing, real-time decisions regarding the data with a light pen or typewriter, and FFTs all of which require only a few minutes per data case. In the following sections the hardware, software and a sample data analysis of EXAFS will be used to demonstrate the program's capabilities.

The program has been developed to analyze digital EXAFS data (see Sayers, Lytle, & Stern, 1971 for examples), but can be used for any other kind of Fourier analysis problem. Data in graphical form may also be analyzed by digitizing first. Most scattering experiments (x-ray, electron, neutron or EXAFS) are conducted so that data are accumulated in equi-spaced angular increments which are not equally spaced in the transform variable. This interpolation is accomplished as a first step in this program, hence any data equi-spaced or not may be analyzed.

1. COMPUTER HARDWARE

The hardware for this program is a System/360 model 65 IBM computer, attached directly to an IBM 2250 vector display scope with a 32-key function keyboard, a standard typewriter type entry keyboard, and a light detecting pen. The scope is similar in appearance to a TV screen. The light detecting pen can be touched directly on the screen yielding the precise coordinates of contact, which can be used both for terminating the data and issuing program instructions. Internal core storage is limited to 280K bytes at our facility because of the multi-processing requirements of the computer. This problem has been reduced by development of an FFT algorithm (Singleton, 1967) which uses a relatively small amount of in-core storage and uses 10 auxiliary mass storage units for data storage. The input data is entered on cards with the program residing on permanent disc storage. Printed output goes on a standard, high-speed printer. Graphical output (hard copies) of any screen display may be obtained on either SC4020 or CALCOMP plotting hardware at the user's option. This output is written on two 7-track tapes to be processed offline. The entire program requires 280K bytes of internal mass storage and operates well in the multi-variable task processing environment.

2. COMPUTER SOFTWARE

The interactive computer graphics program consists of one long driver program that calls numerous subroutines from the IBM 2250 graphics subroutine package (IBM, 1968) and the FFT subroutine. All mathematical manipulation with the exception of the transform is performed by the main program. The IBM-supplied software facilitates communication with the main program in controlling light-pen and function key interrupts, display regeneration, and typed entries.

At our facility core storage for scope jobs is limited to 280K bytes of core which represents a problem since Fourier transforms of 2^{13} complex

2. (Continued)

data pairs must be performed. The graphics subroutine package takes about 170K bytes of storage, leaving only 110K bytes for the main program and the FFT algorithm. Generally, FFT algorithms (Bingham & Godfrey, 1967) need at least 2.5 times the size of the transform for internal storage in order to perform an in-core transform. Since this amount of storage was simply not available for processing in a graphics mode, an algorithm was chosen that uses auxiliary mass storage (Disc Files) (Singleton, 1967). This FFT algorithm occupies only 16K bytes of storage plus 20K bytes for high-speed buffers to perform a double precision transform. All of the routines used including the FFT subroutine were coded in FORTRAN with the exception of certain GSP routines.

3. ANALYSIS PROCEDURE

In order to demonstrate the capabilities of this program, a sample data examination is presented using the K-edge EXAFS from crystalline germanium (Ge). EXAFS is the series of oscillations appearing on the high energy side of x-ray absorption edges. The theory of EXAFS (Sayers, et al., 1971) is given by

$$x(k) = \sum_{j=1}^{n} \frac{N_j}{r_j^2} g(k) \exp(-\alpha^2 k^2) \mathrm{Sin}(2kr_j + 2\eta)$$

where the sum is over the shells of N_j atoms surrounding the absorbing atom at a distance r_j, $g(k)$ is the energy dependence of the scattering of the photo-electron, the exponential is a Debye-Waller type temperature term and η is a phase shift introduced by the absorbing atom. Because of the basic sine wave dependence of $x(k)$ we have shown that Fourier analysis of the data gives peaks located at the atomic distances whose areas are proportional to N_j. This technique has been applied to studies of amorphous semiconductors (Sayers, et al., 1971), catalysts (Lytle, et al., 1974), and charge shielding in metals (Stern & Sayers, 1973).

1. DISPLAY CHI VS K FOR THE DATA JUST READ IN.

2. CHOOSE LIMITS IN K SPACE FOR FOURIER TRANSFORM.

3. DISPLAY CHIBAR VS KBAR FOR THE RANGE TO BE TRANSFORMED AFTER THE DATA HAS BEEN EQUISPACED IN K.

4. MULTIPLY BY CONVERGENCE FACTOR, $A \cdot EXP(-B \cdot k^2)$.

5. PERFORM THE FOURIER TRANSFORM.

6. DISPLAY THE TRANSFORM:

   REAL
   IMAGINARY
   MAGNITUDE

7. MULTIPLY THE TRANSFORM BY Cr^N.

8. SELECT THE LIMITS FOR THE INVERSE TRANSFORM.

9. PERFORM THE INVERSE TRANSFORM.

10. DISPLAY THE INVERSE TRANSFORM.

11. READ THE NEXT DATA CASE.

FIGURE 1 - "Menu" of Program Options

3. (Continued)

One or more decks of Chi versus E (E is the energy above the x-ray absorption edge) are read into the computer. The program displays the "menu" (shown in Figure 1) on the scope listing the analysis options available. Normally analysis proceeds step-by-step returning to the menu after each step; however, if desired, any step may be repeated. The options are shown in the flow chart in Appendix I and are selected by touching the light-pen on the line of the menu desired.

Normally, the first operation is to display the input data with a change of independent variable from energy (E) to the electron wave vector k which is the appropriate Fourier variable and is related to E by

$$k = \left[\frac{2m}{\hbar^2} (E-V_0)\right]^{1/2}$$

where m is the electron mass, $\hbar$ is Planck's constant, and V_0 is an inner potential which defines the zero of kinetic energy.

Pressing either a plot button (for CALCOMP or SC4020 plots) or the CONTINUE button, returns the menu display. At this point select line two of the menu and type the upper and lower transform limits in k with the standard keyboard or press continue and CHI versus k will again appear to allow selection of the data range to be transformed (using the light-pen) or choose any combination of typed limits or light-pen are automatically marked with a "+". This display may be plotted and again the menu returns after either plotting or a continue is pressed. The initial data CHI vs. k for crystalline Ge, with a typical transform range selected by the light-pen is shown in Figure 2.

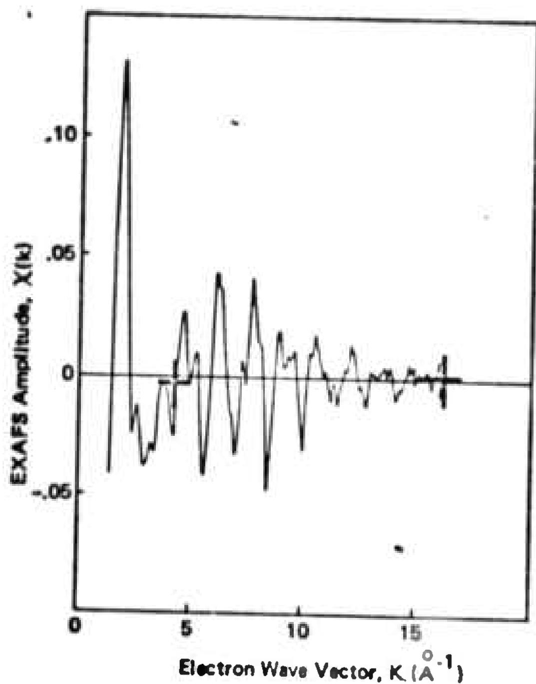

Figure 2 EXAFS amplitude vs. K for crystalline Ge. The "+" marks indicate points selected by the light pen for terminating the function for the transform of Fig. 4.

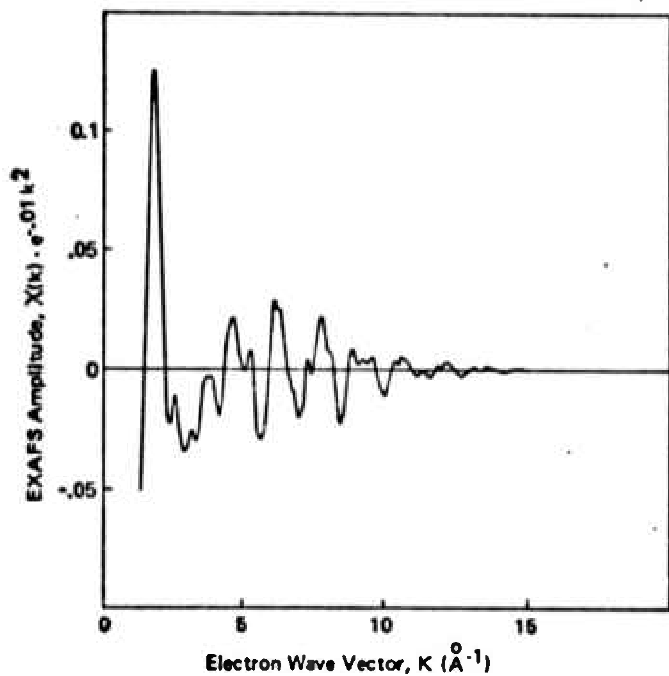

Figure 3 The data of Fig. 2 after a convergence function exp ($-.01K^2$) has been applied.

3. (Continued)

The FFT algorithm requires input data which is equi-spaced in k. This is generated by touching the next line of the menu with the light-pen which uses a parabolic interpolation routine to equi-space the data (Chibar vs. Kbar). The number of points displayed in the range of the transform is proportional to the number of input data points. These points are followed with zeros to provide a total of 2^{13} complex data pairs. There are 400-1000 values of Chibar in a typical transform range and the remaining 7000 or so points are zeros. This technique (Bingham, et al., 1967) is widely used to achieve higher resolution in the transform. By extending the length of the period in k-space through adding zeros, the distance between harmonics (r-space) is reduced. The transform input files are filled and the display for Chibar vs. Kbar (the equi-spaced values of k), appears on the screen. The user has an option of multiplying Chibar by a convergence factor $A \cdot \exp(-B \cdot k^2)$ where default values are A=1 and B=0. A plot of CHIBAR vs. KBAR with a convergence factor (α^2=B=.01) is shown in Figure 3. This data may also be printed on the line printer.

The next line performs the actual transform. While this operation is progressing, the function buttons and scope display are off to save core storage. Typical transforms take about 3 minutes depending on other multiprocessing demand. We are currently improving this version to reduce this time to less than 1 minute. When the transform is complete the menu reappears on the scope and the DISPLAY TRANSFORM option is selected. An option is presented to multiply the transform by Cr^N (default values A=1,N=0). The real part, imaginary part, and magnitude (magnitude = $[(\text{real})^2 + (\text{imag})^2]^{1/2}$ of the Fourier transform between r=0 and 10 Å are consecutively displayed by pressing the plot or continue buttons. This data may also be printed. The real and imaginary part as well as the magnitude of the transform of the data from Figure 3 are shown in Figure 4 where $Cr^N = \pi r^2$.

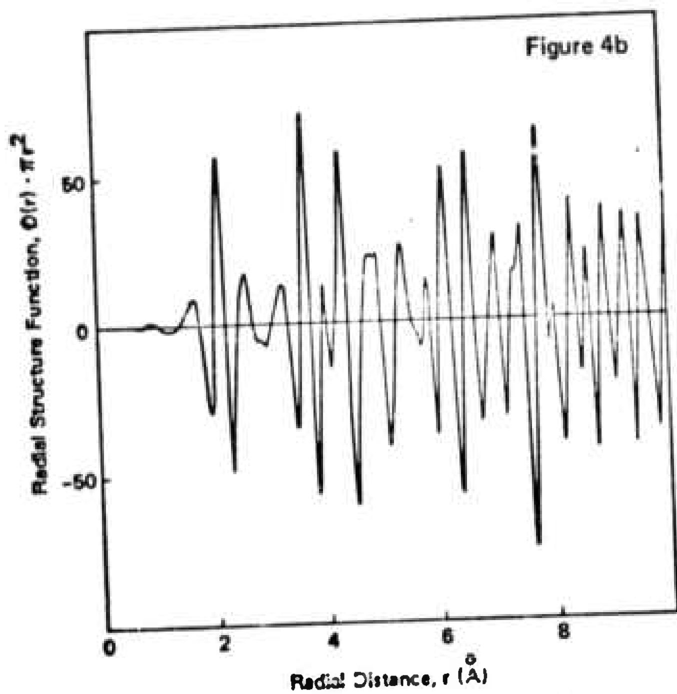
Figure 4b
Radial Structure Function, $\Phi(r) \cdot \pi r^2$
50
0
-50
0
2
4
6
8
Radial Distance, r (Å)

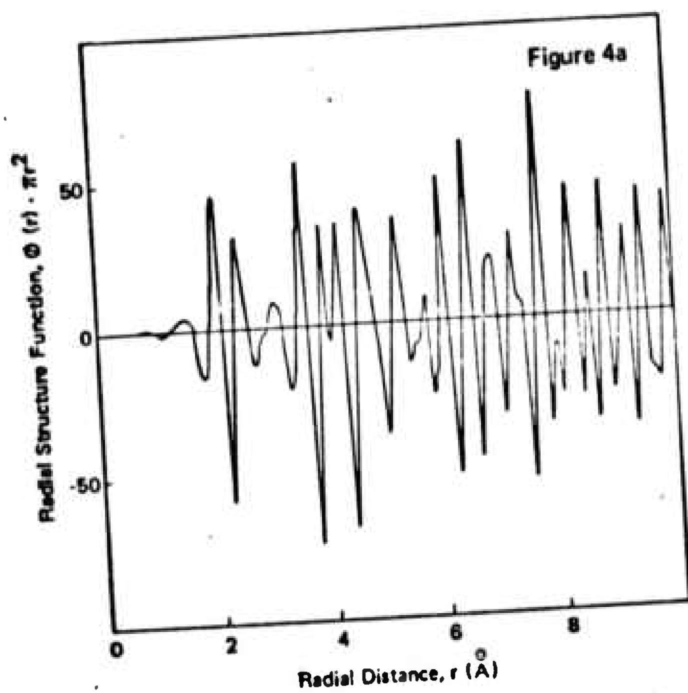
Figure 4a
Radial Structure Function, $\Phi(r) \cdot \pi r^2$
50
0
-50
0
2
4
6
8
Radial Distance, r (Å)

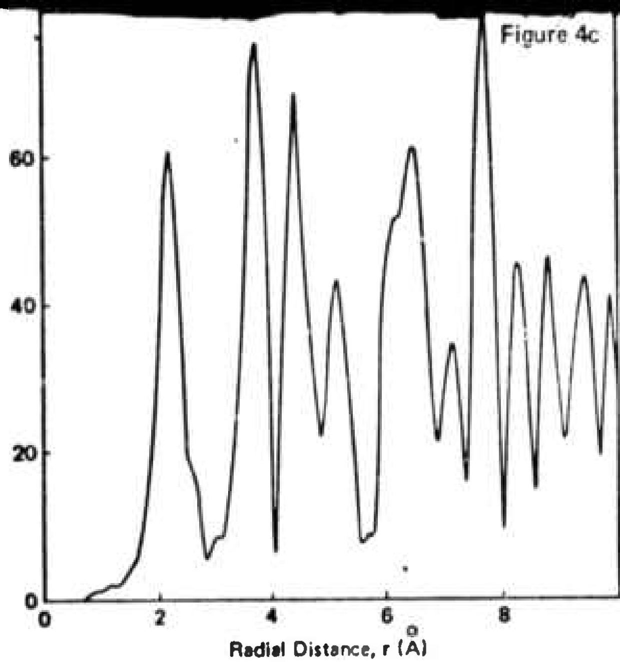

Figures 4a, b and c The real part, imaginary part and magnitude of the FFT for the data of Fig. 2. The vertical scale is proportional to the number of atoms on each coordination shell and has been multiplied by πr^2. The horizontal scale is the radial distance from the absorbing atom in Å.

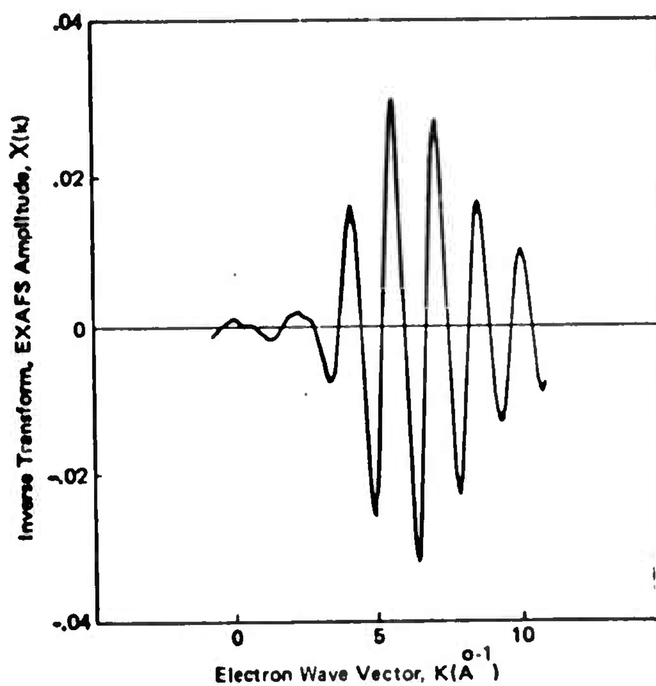

Figure 5 The inverse FFT for the first peak in Fig. 4c for $1.49 < r < 2.81$ Å plotted EXAFS amplitude vs radial distance, r.

3. (Continued)

After completion of this step the menu is displayed again on the screen. The options on lines 8-10 allow all or part of the transform in r-space to be Fourier transformed back to k-space. This is very useful in structural analysis and other applications because it allows the contribution of a particular feature or range in r-space to be studied in k-space without interference from other features. From line 8 of the menu, the range of data to be inverse transformed is selected using the typewriter or light-pen as was done with the initial transform. All data below the lower limit in r and above the upper limit in r are set to zero. No interpolation is needed because the data from the original transform is equi-spaced in r. Selection of the next line performs the inverse transform just as was done previously, and the next line of the menu displays the result. Figure 5 shows the result of isolating a peak in r-space (the first peak in Figure 4C) and subsequent inverse Fourier transformation. This shows what part of the signal Chi vs. k contributed to the selected peak in r-space. A comparison of Figure 5 and Figure 2 shows which features in the original data can be identified with the first peak.

If no other inverse transforms are required, the user has the option of taking another transform over a different range of the data, multiplying by a convergence factor, or multiplying the transform by Cr^N or going on to the next data case. The sample run which has been illustrated here would take less than 10 minutes in actual time on the computer so that several cases per hour can be analyzed.

We have found this program invaluable as an aid for processing EXAFS data. This interactive program package is available for general use at Boeing Computer Services, Inc., Seattle, Washington. From our experience we have found certain operations which are well known in advance and repetitious in nature. These problems are handled with a similar batch program which does not require user interaction. This program is also available.

---

* Research supported in part by the Advanced Research Projects Agency and monitored by the U.S. Army Research office under Contract DAHC04-71-C0010.

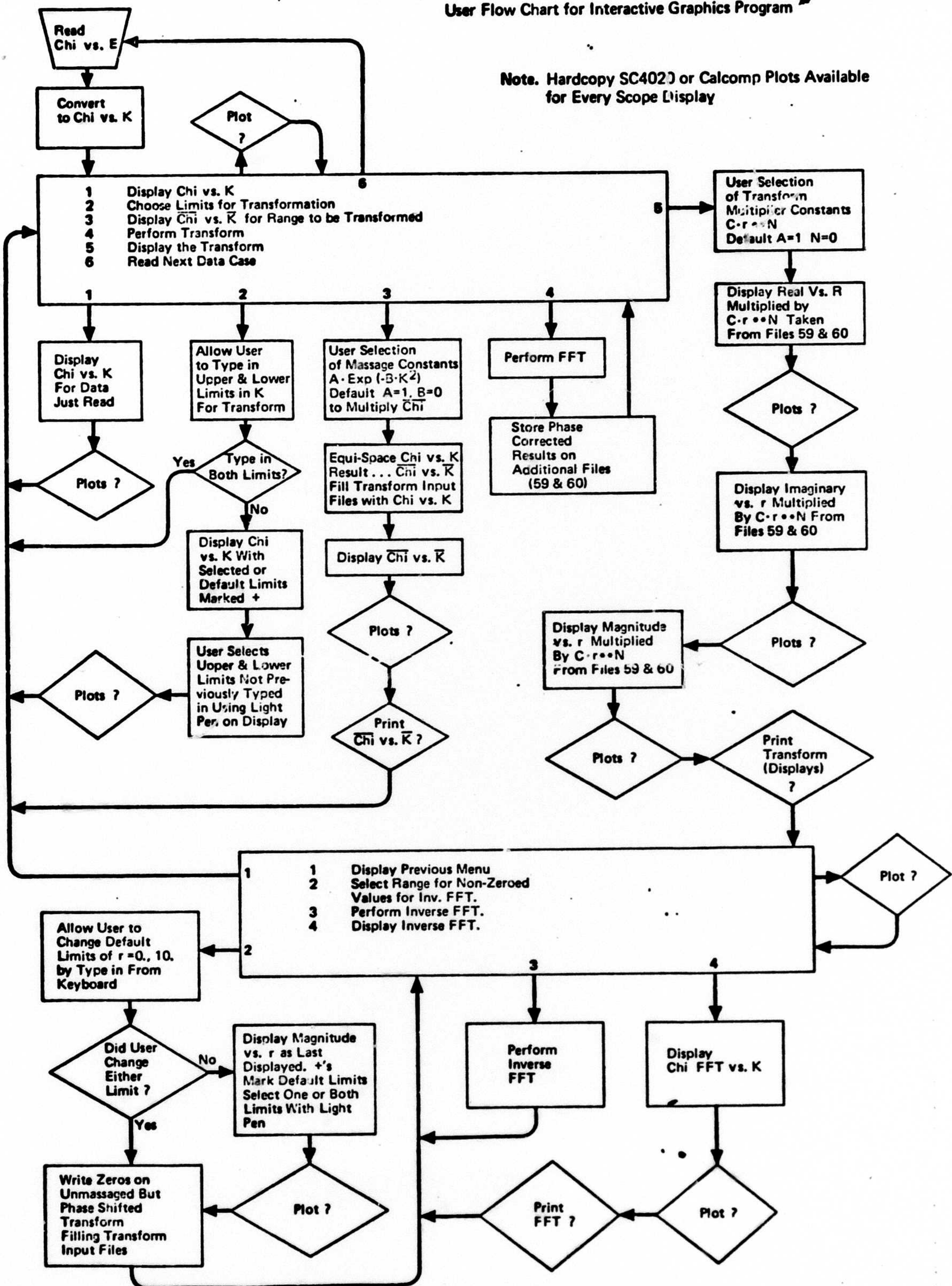

User Flow Chart for Interactive Graphics Program
Note. Hardcopy SC4020 or Calcomp Plots Available for Every Scope Display
Read Chi vs. E
Convert to Chi vs. K
Plot ?
1 Display Chi vs. K
2 Choose Limits for Transformation
3 Display Chi vs. K for Range to be Transformed
4 Perform Transform
5 Display the Transform
6 Read Next Data Case
User Selection of Transform Multiplier Constants C·r••N Default A=1 N=0
Display Real Vs. R Multiplied by C·r••N Taken From Files 59 & 60
Plots ?
Display Chi vs. K For Data Just Read
Plots ?
Allow User to Type in Upper & Lower Limits in K For Transform
Type in Both Limits?
Yes
No
Display Chi vs. K With Selected or Default Limits Marked +
User Selects Upper & Lower Limits Not Previously Typed in Using Light Pen on Display
Plots ?
User Selection of Massage Constants A·Exp (-B·K2) Default A=1, B=0 to Multiply Chi
Equi-Space Chi vs. K Result . . . Chi vs. K Fill Transform Input Files with Chi vs. K
Display Chi vs. K
Plots ?
Print Chi vs. K ?
Perform FFT
Store Phase Corrected Results on Additional Files (59 & 60)
Display Imaginary vs. r Multiplied By C·r••N From Files 59 & 60
Plots ?
Display Magnitude vs. r Multiplied By C·r••N From Files 59 & 60
Plots ?
Print Transform (Displays) ?
1 Display Previous Menu
2 Select Range for Non-Zeroed Values for Inv. FFT.
3 Perform Inverse FFT.
4 Display Inverse FFT.
Plot ?
Allow User to Change Default Limits of r=0., 10. by Type in From Keyboard
Did User Change Either Limit ?
No
Yes
Display Magnitude vs. r as Last Displayed. +'s Mark Default Limits Select One or Both Limits With Light Pen
Plot ?
Write Zeros on Unmassaged But Phase Shifted Transform Filling Transform Input Files
Perform Inverse FFT
Display Chi FFT vs. K
Plot ?
Print FFT ?

REFERENCES

1. Bingham, C., Godfrey, M. D., and Tukey, J. W. (1967). IEEE Trans. Audio and Electroacoustics. AU-15,2,56-66.

2. Cooley, J. W. and Tukey, J. W. (1965). Maths Comput. 19, 297-301.

3. IBM Systems Reference Library (1968). IBM System/360 Operating System Graphic Subroutine Package [GSP] for FØRTRAN IV, CØBØL, and PL/1. form C27-6932-3.

4. Lytle, F. W., Sayers, D. E. and Moore, E. B. (1974). Appl. Phys. Lett. Jan. 15, 1974.

5. Sayers, D. E., Lytle, F. W., and Stern, E. A. (1971). Phys. Rev. Lett. 27, 1204, J. Non-Cryst. Solids 8-10, 401 (1972).

6. Singleton, R. C. (1967). IEEE Trans. Audio and Electroacoustics. AU-15,2,91-98.

7. Stern, E. A. and Sayers, D. E. (1973). Phys. Rev. Lett. 30, 174.